MCB
Journals.ASM.org

MacroH2A1 Regulates the Balance between Self-Renewal and Differentiation Commitment in Embryonic and Adult Stem Cells

Catherine Creppe,[a] Peggy Janich,[b] Neus Cantariño,[a] Marc Noguera,[a] Vanesa Valero,[a] Eva Musulén,[c] Julien Douet,[a] Melanija Posavec,[a] Juan Martín-Caballero,[d] Lauro Sumoy,[a] Luciano Di Croce,[b,e] Salvador A. Benitah,[b,e] and Marcus Buschbeck[a]

Institute for Predictive and Personalized Medicine of Cancer (IMPPC), Badalona, Spain[a]; Centre de Regulació Genòmica, Barcelona, Spain[b]; Hospital Universitari Germans Trias i Pujol, Badalona, Spain[c]; Parc de Recerca de Biomèdica Barcelona, Barcelona, Spain[d]; and Institució Catalana de Recerca i Estudis Avançats (ICREA), Barcelona, Spain[e]

One of the most striking epigenetic alterations that occurs at the level of the nucleosome is the complete exchange of the canonical H2A histones for the macroH2A variant. Here, we provide insight into the poorly recognized function of macroH2A in transcriptional activation and demonstrate its relevance in embryonic and adult stem cells. Knockdown of macroH2A1 in mouse embryonic stem (mES) cells limited their capacity to differentiate but not their self-renewal. The loss of macroH2A1 interfered with the proper activation of differentiation genes, most of which are direct target genes of macroH2A. Additionally, macroH2A1-deficient mES cells displayed incomplete inactivation of pluripotency genes and formed defective embryoid bodies. *In vivo*, macroH2A1-deficient teratomas contained a massive expansion of malignant, undifferentiated carcinoma tissue. In the heterogeneous culture of primary human keratinocytes, macroH2A1 levels negatively correlated with the self-renewal capacity of the pluripotent compartment. Together these results establish macroH2A1 as a critical chromatin component that regulates the delicate balance between self-renewal and differentiation of embryonic and adult stem cells.

Chromatin and its alterations provide the molecular basis for the epigenetic memory of a cell. During cell fate transitions, such as differentiation and development, chromatin modifications need to be removed and new ones set in a highly concerted manner (22). During the past years, we have begun to understand how this is achieved for many of the posttranslational modifications of the histone tails and the DNA itself. However, remarkably little is known about the role and regulation of a much more extensive chromatin alteration, namely, that of exchanging a canonical histone for a variant protein. Numerous histone variants exist for the histones H3 and H2A (39). Among these, macroH2A stands out because of its unique size and domain structure. A C-terminal linker connects the histone fold domain of macroH2A to a macro domain. This domain protrudes from the compact structure of the nucleosome and is likely to affect the function and organization of the surrounding chromatin (11). Three different proteins, termed macroH2A1.1, macroH2A1.2, and macroH2A2, are generated from two genes and alternative splicing of the primary macroH2A1 mRNA (reviewed in reference 7). Unless specified, we will refer to these as macroH2A (for all three forms) or macroH2A1 (for macroH2A1.1 and macroH2A1.2).

In embryonal carcinoma cells, both macroH2A1 and macroH2A2 localize to developmental genes (10). A similar genomic distribution for macroH2A1 was confirmed in human fibroblasts and breast cancer cells (19). MacroH2A occupancy generally correlates with gene repression and low transcriptional activity (10, 19). Accordingly inhibiting macroH2A increased the transcription levels, or facilitated the activation, of target genes (1, 10, 12, 23). The view of macroH2A as a pure repressor was challenged by two groups reporting that the presence of macroH2A1 was essential for activating genes in response to stimuli such as heat shock or serum deprivation (19, 35). The physiological relevance of macroH2A function is best illustrated *in vivo*, where macroH2A was required for proper zebrafish development (10). In lung and breast cancer, loss of macroH2A1.1 and macroH2A2 correlated with poor prognosis (40). In addition, in melanoma, loss of macroH2A1 and macroH2A2 promoted progression to a metastatic state (27). At present, it is not understood which biological functions of macroH2A depend on its repressive function and which on its activating capacity.

Here, we provide insight for the role of macroH2A in embryonic and adult stem cells. We found that in ES cells macroH2A1 regulates the crucial balance between self-renewal and differentiation commitment, acting on the side of differentiation. We further demonstrate that it is the newly recognized function of macroH2A in transcriptional activation by which macroH2A promotes differentiation. This new role for macroH2A seems not to be limited to ES cells, as we also have observed similar effects in the pluripotent cell compartment of primary human keratinocytes.

MATERIALS AND METHODS

Antibodies and plasmids. We used the antibodies against tubulin and the anti-Flag M2 from Sigma-Aldrich, H3 C-terminal, H3K27me3, H3K4me2, and H3K4me3 from Upstate, EZH2 (36), Ki67 from BD Pharmingen, Oct3/4 from BD Pharmingen, involucrin from AbCam, S100, GFAP, and the cytokeratin clones AE1/AE3 from DakoCytomation, macroH2A1.1 (40), and macroH2A1 and macroH2A2 (10). Expression plasmids and pLKO-1 constructs were generated with standard PCR and cloning techniques. pRetroSUPER constructs were described previously (10).

Cell culture and gene transfer. The mouse ES cell line E14 (25) was maintained in minimal essential medium (MEM) (Sigma) supplemented with 20% fetal bovine serum (FBS) (HyClone), 1% penicillin-streptomycin, 1% GlutaMAX, 1% nonessential amino acids, 1% sodium pyruvate, and

Received 22 September 2011 Returned for modification 21 October 2011
Accepted 26 January 2012
Published ahead of print 13 February 2012
Address correspondence to Marcus Buschbeck, mbuschbeck@imppc.org.
Supplemental material for this article may be found at http://mcb.asm.org/.

doi:10.1128/MCB.06323-11

0.2% β-mercaptoethanol, in the presence of leukemia inhibitory factor (LIF) corresponding to 1,000 U/ml. The cells were propagated every 2 days by trypsinizing and plating onto 0.1% gelatin-coated plates, with a split ratio of 1:8. Primary human keratinocytes (PHKs), isolated from adult foreskin, were grown on mitomycin C-treated J2-3T3 feeder cells in FAD medium (1 part Ham's F-12 medium, 3 parts Dulbecco MEM [DMEM], 1.8×10^{-4} M adenine) supplemented with 10% fetal bovine serum, 0.5 μg/ml hydrocortisone, 5 μg/ml insulin, 10^{-10} M cholera toxin, and 10 ng/ml epidermal growth factor (EGF). J2-3T3 cells were previously expanded in DMEM containing 10% donor bovine serum and treated with 4 μg/ml mitomycin C (Sigma) for 2 h. For the colony formation assay, 10^3 PHKs were seeded per well in a six-well plate on top of a layer of J2-3T3 cells. At the end of the experiment, cells were stained with crystal violet. HEK293T and GP2 cells were cultivated in DMEM supplemented with 10% FCS. Retroviral and lentiviral infections were performed essentially as described previously (2, 8). For suppression of macroH2A1, cells were infected with vectors expressing either specific or control small hairpin RNAs and selected with 2 μg/ml puromycin.

Stem cell differentiation and teratoma formation. For neuronal differentiation, 1 μM retinoic acid was added directly to the plates in LIF-free medium. Replating assays were performed in analogy to experiments described elsewhere (17). For embryoid body (EB) formation, 10^3 cells were seeded in 20-μl hanging drops on petri dish lids and grown in the absence of LIF. After 48 h, EBs were collected and grown in suspension in noncoated petri dishes. The medium was changed every 2 days until harvest. For teratoma formation, we injected 200 μl phosphate-buffered saline (PBS)–25% Matrigel containing 1×10^6 mES cells subcutaneously in both laterals of Swiss nude mice. All of the teratomas analyzed were localized at the site of injection, and none of them showed any signs of invasion or metastasis at the time of being sacrificed. They did not appear to affect the health of the host mice.

Protein analysis. Lysis and Western blot analyses were performed as previously described (9, 42). Immunohistochemistry and immunofluorescence on paraffin-embedded sections were performed as described previously (5, 24). For the separation of nucleosolic and chromatin fractions, we have used a modified version of the Dignam protocol. In brief, isolated nuclei were resuspended in low-salt buffer (20 mM HEPES, pH 7.9, 1.5 mM $MgCl_2$, 0.2 mM EDTA, 20 mM KCl, 25% [wt/vol] glycerol, 0.5 mM dithiothreitol [DTT]). The soluble nucleosolic fraction was extracted during 30 min of constant moderate agitation after addition of 1 volume of high-salt buffer (20 mM HEPES, pH 7.9, 1.5 mM $MgCl_2$, 0.2 mM EDTA, 800 mM KCl, 25% [wt/vol] glycerol, 1% NP-40, 0.5 mM DTT). Chromatin was pelleted by ultracentrifugation for 1.5 h at $\geq 200{,}000 \times g$.

Analysis of gene expression and enriched chromatin fractions. Following the supplier's instructions, RNA was purified from 2×10^6 cells using the Qiagen RNeasy minikit, with a DNase 1 digestion step to avoid any potential DNA contamination. Total RNA (1 μg) was reverse transcribed using a cDNA synthesis kit (Roche) and oligo(dT) primers. Relative cDNA levels were quantified by quantitative PCR (qPCR). Values were normalized to the expression of two housekeeping genes (*Rpo* and *Gapdh* for mES cells and *HPRT* and *GAPDH* for keratinocytes). Chromatin immunoprecipitation (ChIP) experiments were performed and analyzed essentially as previously described (18). The sequences of all oligonucleotides used here are provided as additional material at http://tinyurl.com/buschbeck-lab. Results cited as data not shown are also available on the group's homepage. Unless indicated otherwise, ChIP results are given as the percentage of ChIP relative to the input material. For ChIP sequencing (ChIP-seq), 10 ng of DNA was enriched by ChIP and quantified with the PicoGreen fluorescence method. Library generation and direct massive parallel sequencing on an Illumina genome analyzer were performed according to the suppliers' instructions.

Data analysis and statistics. Reads of 36 bp were mapped onto the mouse genome (*Mus musculus* reference strain NCBIM37/mm9; UCSC) using the Bowtie short read aligner (version 0.11.3) (28); a maximum of 2 mismatches and a 28-bp seed size were allowed. Only reads mapping to a single position in the genome were used. The MACS software (v 1.3.6.1) (44) was used for peak calling for the H3K4 and H3K27 reads, and the CCAT software (v 2.0) (43) for the macroH2A reads, with a sliding window size of 1,000 bp using the IgG signal as background. The R/BioConductor (20) ChIPPeakAnno, and biomaRt packages were used to annotate (15, 45). Genes were considered to be targets if their peak overlapped with the gene body or with the 10-kb upstream promoter region. The DAVID functional cluster analysis was used to annotate functionally related groups of genes (26). For the correlation of ChIP data with gene expression, transcripts were grouped in categories 0 (no signal) and 1 (very low) to 5 (high) according to the spot intensity of corresponding probes on Agilent human expression arrays generated by Morey and colleagues (31).

Unless indicated otherwise, error bars represent the standard deviations and asterisks represent $P < 0.05$, as calculated with two-tailed *t* tests. For nonparametric distributions, *P* values were determined by the Mann-Whitney test.

Microarray data accession number. Data from the ChIP-seq analysis have been deposited in the Gene Expression Omnibus under accession number GSE35087.

RESULTS

MacroH2A1.2 occupies differentiation genes in mouse ES cells. We set out to assess the relative expression levels of all macroH2A forms in self-renewing mouse E14 ES cells. On the protein level, macroH2A1 is expressed to a greater level than macroH2A2 (Fig. 1A). Quantifying the relative abundance of mRNA, we found that mES cells contained 7 times more messenger for macroH2A1 than macroH2A2 (Fig. 1B). Moreover, all of the macroH2A1 mRNA encoded the splice variant macroH2A1.2 (Fig. 1B). This could be further confirmed by taking advantage of a unique restriction site in one of the two mutually exclusive exons of the macroH2A1 splice variants (Fig. 1C). Since these data suggested that the macroH2A1.2 form constitutes more than 80% of all cellular macroH2A, we decided to focus on this isoform by using an antibody that was generated against its macro domain (10). We enriched macroH2A1-bound chromatin from mES cells by chromatin immunoprecipitation and analyzed the coprecipitated DNA by direct massive parallel sequencing. Nonspecific IgG was included as a negative control.

We were able to unequivocally map around 15 and 12 million sequences for macroH2A1 and IgG, respectively, to the mouse reference genome. Using a sliding window of 1,000 bp and IgG as a background control, we identified a total of 2,560 macroH2A1-enriched regions (for more detail, see File S1 in the supplemental material). Since the ChIP-seq analysis was not saturated, these 2,560 have to be considered a sample of macroH2A-enriched chromatin rather than a comprehensive description. Around 25% of all these peaks overlapped with annotated 494 genes or with their 10-kb promoter regions (Fig. 1D). Zooming in on the transcriptional start sites (TSS) of these target genes, we found a minimum of macroH2A occupancy at the immediate TSS (Fig. 1E). Genes with increasing expression levels were progressively underrepresented among macroH2A1 target genes (Fig. 1F). Next, we used DAVID functional cluster analysis (26) to annotate functionally related groups of genes that are enriched for macroH2A1 in mES cells. Several of the top-scoring clusters were directly related to the regulation of developmental processes (Fig. 1G; see also File S1). These clusters contain many genes that are relevant for cell differentiation, including those that encode secreted ligands (such as Wnt8a), cell surface receptors (such as FGFR1), and transcription factors (such as Pax3).

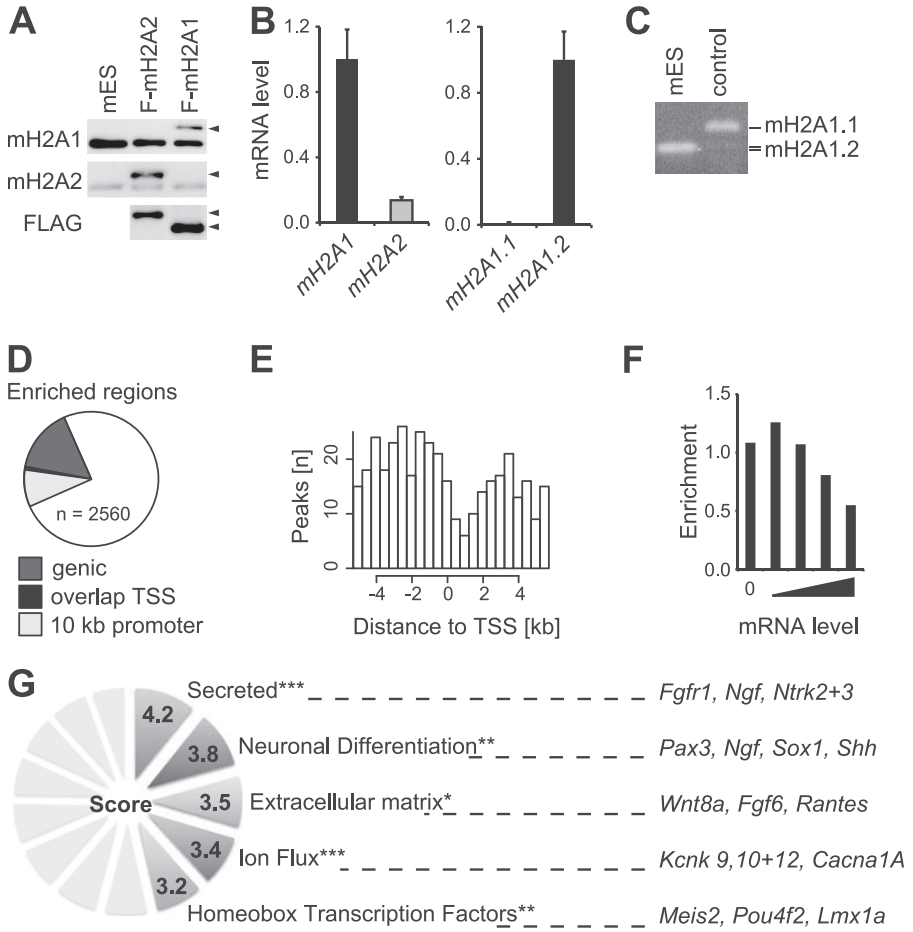

FIG 1 MacroH2A1.2 is enriched on genes that regulate differentiation in ES cells. (A) Lysates from E14 mouse embryonic stem (mES) cells were analyzed by Western blotting together with extracts containing similar amounts of Flag (F)-epitope-tagged macroH2A1.2 and macroH2A2 (marked with arrowheads). (B) The relative mRNA levels of macroH2A forms were analyzed by quantitative RT-PCR and normalized to two housekeeping genes and equimolar reference samples. (C) MspI restriction fragment length polymorphism analysis of an RT-PCR product spanning the variant exon allows the macroH2A1 splice forms to be distinguished. Murine cells expressing exclusively macroH2A1.1 were included as control. (D) Enriched regions (peaks) of macroH2A1 identified by massive parallel sequencing of DNA immunoprecipitated by anti-macroH2A1 from chromatin are shown in respect to annotated genes. (E) The positions of the peaks shown in panel D were plotted against annotated transcription start sites (TSS). (F) Correlation of mH2A1 occupancy with the transcriptional level. Genes were grouped into five expression categories according to probe intensities on Agilent Expression arrays (0, no signal/expression; 1 to 4, very low to high expression). (G) DAVID functional annotation cluster analysis of macroH2A1 target genes. All clusters with an enrichment score of >2 are represented. Asterisks indicate the *P* value of the top-ranked component of each cluster: *, $P < 10^{-4}$; **, $P < 10^{-5}$; and ***, $P < 10^{-6}$. Gene examples are given at the right. For more details on panels D to G, see File S1 in the supplemental material.

MacroH2A1 is required for a full response to neuronal differentiation. Since neuronal differentiation was among the top functional clusters that were annotated for macroH2A1 target genes (Fig. 1G), we decided to initially focus our attention on this process. Neuronal differentiation of mouse ES cells can be induced by the addition of retinoic acid (RA) (21). In accordance with the previous observation that macroH2A1 is upregulated upon differentiation of stem cells (14, 38), we found that the addition of RA resulted in an increase of macroH2A1.2 on the protein and RNA levels (Fig. 2A and B). The macroH2A1.2 level directly dictates the loading of macroH2A1.2 onto chromatin, as no macroH2A1 could be detected in the nucleosol (data not shown). MacroH2A1.1 and macroH2A2 are also increased upon treatment with RA but remain expressed at much lower levels than macroH2A1.2 (Fig. 2B). We next analyzed the occupancy of macroH2A in self-renewing and differentiating cells on a panel of target genes by chromatin immunoprecipitation (ChIP). We focused our attention on genes known to be involved in differentiation, including *Pax3*, *Msx1*, and *Hand1*. We could confirm the enrichment of macroH2A1 on these genes in respect to housekeeping genes and genes that encode the core pluripotency-maintaining transcription factors Oct4, Nanog, and Sox2 (Fig. 2C). Concomitant with the RA-induced increase in macroH2A1 expression, macroH2A1 occupancy was augmented during neuronal differentiation on almost all target genes (Fig. 2C). The same held true for the less highly expressed macroH2A2 (data not shown). Next, we had a closer look at *Pax3* as one of the macroH2A1 target genes. RA-induced Pax3 transcription cooccurred with increased loading of macroH2A1 that was most pronounced at TSS distal regions of the upstream promoter and the transcribed region (Fig. 2D).

To test whether macroH2A is required for the proper response of differentiation genes, we used two different short hairpin RNAs (shRNAs) directed against the shared part of macroH2A1 splice

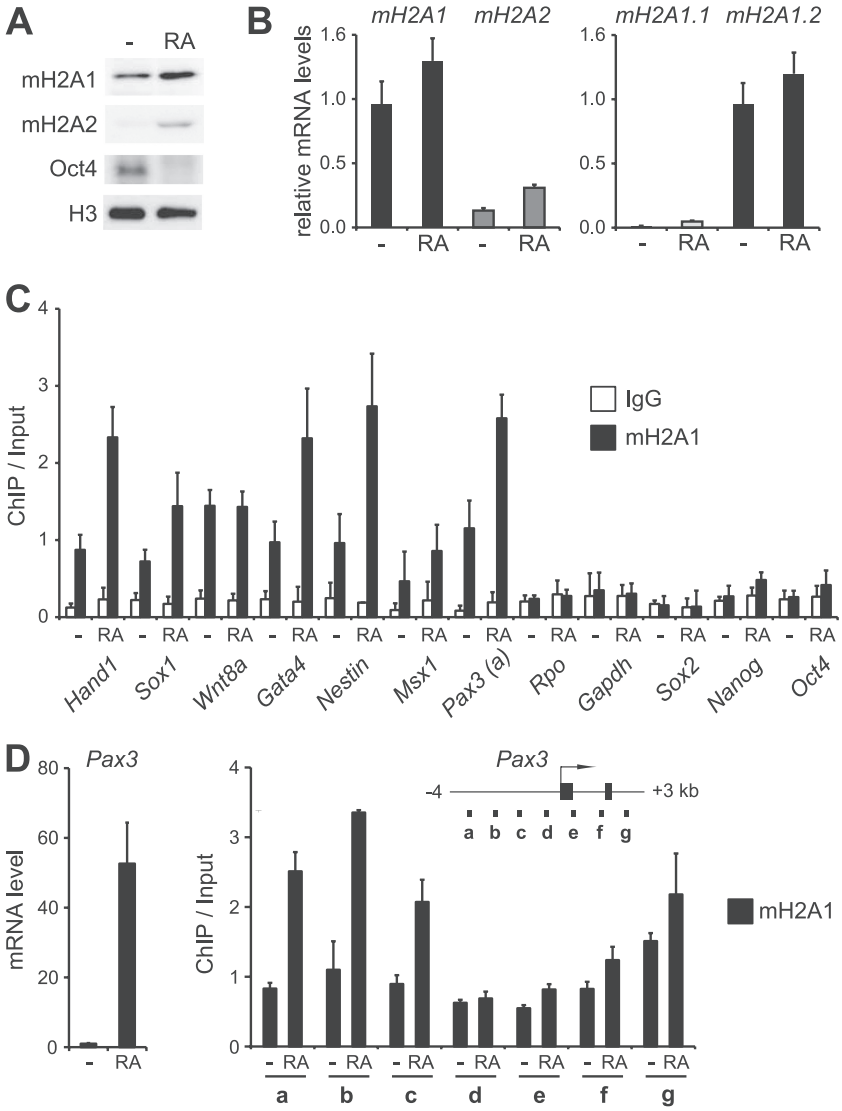

FIG 2 MacroH2A is retained on its target genes upon induction of neuronal differentiation. Cells were treated with 1 μM retinoic acid (RA) for 3 days. (A) Western blot analysis of macroH2A1 and macroH2A2 in total nuclei. Oct4 was included as a differentiation control, and histone H3 was used as a loading control. (B) The relative mRNA levels of total macroH2A1, macroH2A2, and the splice variants macroH2A1.1 and macroH2A1.2 were analyzed by quantitative RT-PCR and normalized to two housekeeping genes and equimolar reference sampled. (C) The occupancy of macroH2A1 on genes was analyzed by chromatin immunoprecipitation (ChIP) in self-renewing cells and differentiating cells treated with 1 μM RA for 3 days. Error bars denote standard deviation, and $n = 3$. (D) The mRNA level of Pax3 and the occupancy by macroH2A1 around the transcription start site of Pax3 were analyzed by quantitative RT-PCR and ChIP, respectively. Error bars denote standard deviation, and $n = 3$.

variants. Both shRNAs efficiently repressed macroH2A1 expression even after 3 days of RA treatment (Fig. 3B), and no compensation by macroH2A2 occurred (data not shown). Importantly, this strong reduction of macroH2A levels did not affect proliferation or survival of mES cells (data not shown). As shown in Fig. 3A, loss of macroH2A1 significantly reduced the RA-induced activation of its target genes involved in differentiation, including *Pax3*, *Msx1*, and *Hand1*, although it did not affect basal transcription levels in self-renewing stem cells. The RA nonresponsive genes *Upp1*, *Srcap*, and *Hmg20A* were not affected by the knockdown of macroH2A1. Activation of differentiation genes is known to trigger several negative feedback mechanisms that contribute to the inactivation of core pluripotency factors; this inactivation is required for the proper execution of the differentiation program (reviewed in reference 33). As expected, addition of RA reduced the mRNA levels of the three main pluripotency regulators, *Nanog*, *Oct4*, and *Sox2* (Fig. 3A). However, the repression of those factors is less efficient in mH2A1-deficient mES cells, resulting in abnormally high expression of pluripotency transcription factors in those cells compared to that in control cells after RA-induced differentiation (Fig. 3A). In line with this, Oct4 protein could be detected in sh-macroH2A1 cells but not control cells when treated with RA (Fig. 3B). Next, we tested the pluripotency retained by the cells after 6 days of differentiation. In control cells and cells defective for macroH2A, *Oct4* RNA levels are very low after 6 days of RA treatment. When RA medium is replaced by ES cell maintenance medium, control cells maintain very low levels of *Oct4* expression while macroH2A-deficient mES cells show a significant increase of *Oct4* mRNA.

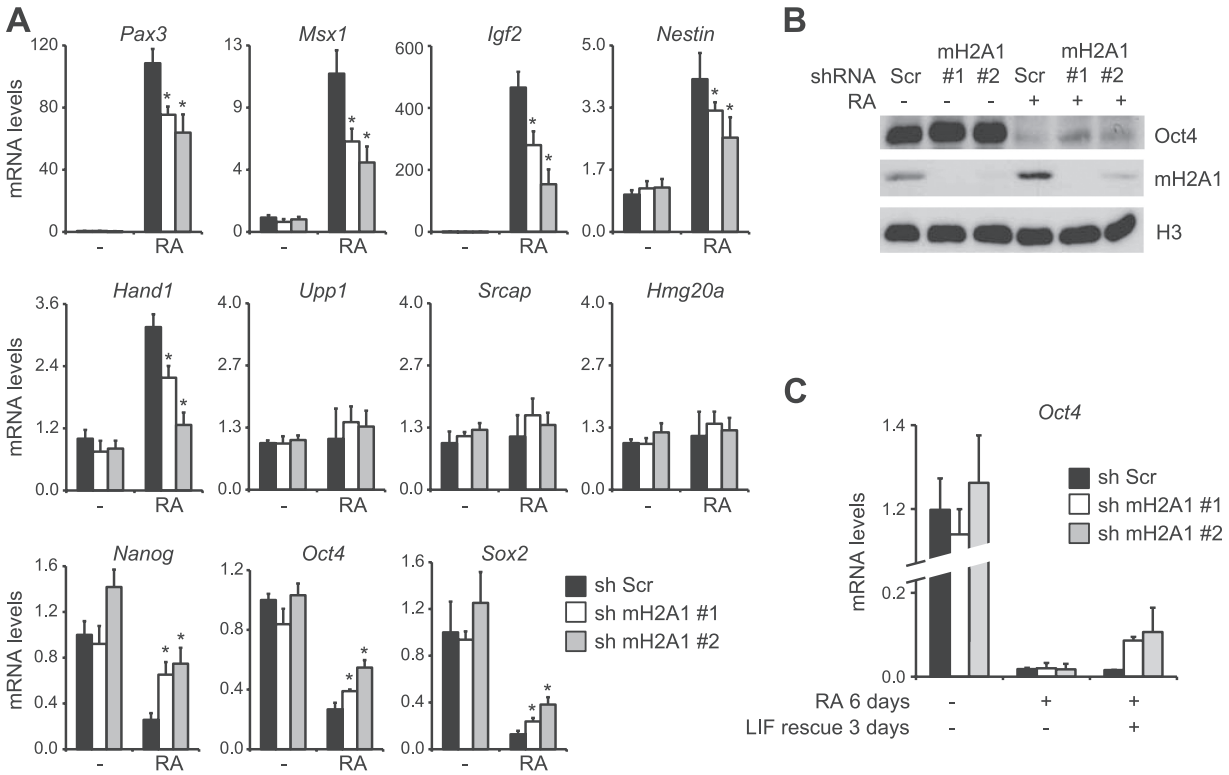

FIG 3 Depletion of macroH2A1 interferes with the neuronal differentiation of mES cells. (A) Expression levels of differentiation and pluripotency genes were analyzed by RT-qPCR in mES cells that were untreated or treated with 1 μM RA for 3 days. *Upp1*, *Srcap*, and *Hmg20a* were included as controls. Error bars denote standard deviation; $n = 3$; *, $P < 0.05$. (B) Crude cell lysates were analyzed by Western blotting using anti-Oct4, macroH2A1, and histone H3 antibodies. (C) mES cells were treated with 1 μM RA for 6 days, after which RA medium was removed and replaced by LIF maintenance mES cell medium. Cells were collected and subjected to RNA extraction and quantitative RT-PCR (17). Error bars denote the variances of results from two independent experiments.

MacroH2A1 is critical for proper embryoid body formation. We next asked whether macroH2A influences only neuronal differentiation or if macroH2A can also affect other lineages. To address this, we decided to study the function of macroH2A1 during embryoid body formation. Embryoid bodies (EBs) provide an *in vitro* model that recapitulates the early differentiation steps of embryonic development (16). During EB formation, ES cells diverge and enter into differentiation programs of all three lineages: ectoderm, endoderm, and mesoderm. Similarly to what was observed during RA-induced differentiation, the levels of macroH2A1.2 increased during EB formation, and macroH2A1.2 accounted for the bulk amount of cellular macroH2A at all time points (data not shown). To study the role of macroH2A1 during the differentiation of mES cells into EBs, we initially used the ES cells that stably expressed shRNA mH2A1#1, which resulted in stable reduction of macroH2A1 throughout the process of EB formation (Fig. 4A and B). In analogy to our previous results with RA treatment, no compensatory upregulation of macroH2A2 was observed (Fig. 4B). As shown in Fig. 4C, EBs generated from sh-macroH2A1 cells and control cells showed phenotypical differences that were most pronounced at late stages of EB formation, as shown for day 8. MacroH2A1-deficient EBs were smaller and showed less of the typical cavitation of late-stage EBs than control EBs. Semiquantitative analysis of mRNA levels demonstrated that EBs derived from sh-macroH2A1 cells retained abnormally high levels of *Nanog*, *Oct4*, and *Sox2* expression at late stages (Fig. 4D). Aberrantly high levels of Oct4 in EBs at day 9 could also be observed on the protein level (Fig. 4A). The activation of differentiation genes of all embryonic lineages was partially impaired in the absence of macroH2A1 (Fig. 4D), with the activation not being fully achieved (for *T/Brachyury*, *Cdx2*, and *Hand1*), delayed (for *GATA4* and *nestin*), or both (for *Pax3*). Finally we tested additional shRNAs for macroH2A1 and macroH2A2 on a representative differentiation and pluripotency gene in late-stage EBs. All four macroH2A-specific shRNAs tested significantly increased the levels of *Nanog* (Fig. 4E). Both macroH2A1-specific shRNAs further reduced the levels of *Gata4* at day 6 of the EB formation process, while shRNAs directed against macroH2A2 did not. It is interesting to note that some of the shRNAs for macroH2A1 or macroH2A2 also reduced the respective other mRNA.

The presence of macroH2A1 on the promoters of differentiation genes whose activation is partially impaired by the suppression of macroH2A1 expression suggested a direct mechanism. MacroH2A1 target genes partially but significantly overlapped with genes marked by trimethylation of lysine 27 alone or in combination with active lysine 4 methylation (data not shown). Since depletion of macroH2A1 did not affect significantly the level of either histone methylation on its target genes (data not shown), at the present we can exclude a defect in the maintenance of these so-called bivalent domains as a possible mechanism.

MacroH2A-deficient teratomas show a massive expansion of immature carcinoma tissue. We next analyzed the impact of macroH2A on the differentiation of mES cells in xenografts. When injected into immunosuppressed mice, mES cells form teratomas,

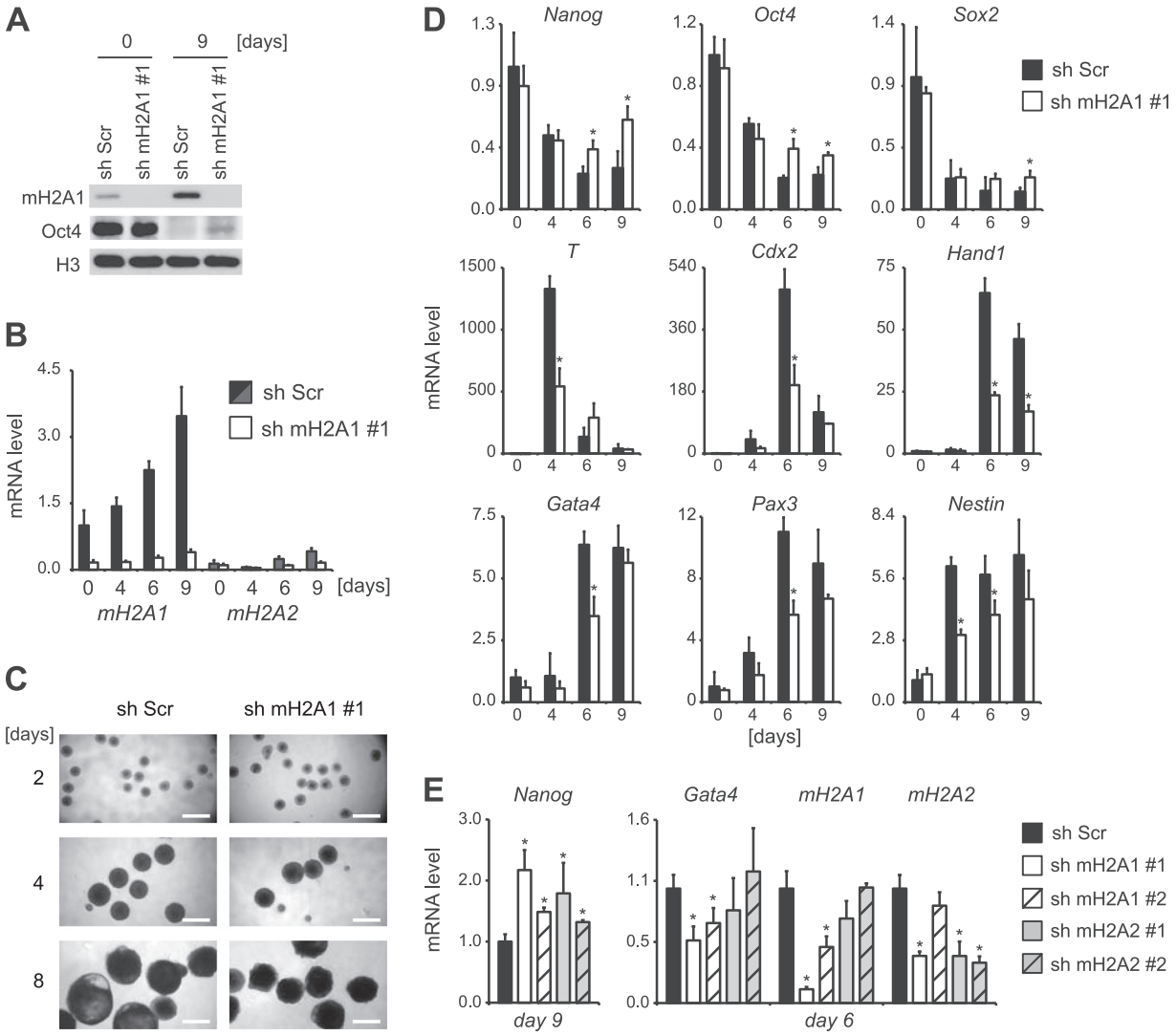

FIG 4 Depletion of macroH2A1 interferes with proper embryoid body formation. (A) Western blot analysis of macroH2A1 and Oct4 in self-renewing mES cells and in embryoid bodies (EBs) at day 9. Histone H3 was used as loading control. (B) The mRNA levels of macroH2A1 and macroH2A2 in control cells and after shRNA-mediated knockdown of macroH2A1 were analyzed at different time points of EB formation and normalized to equimolar reference samples. Error bars denote standard deviation; $n = 3$; *, $P < 0.05$. (C) Light microscopic analysis of EBs revealed that the normal shapes and sizes are perturbed in macroH2A1-deficient cells. Scale bar, 500 μm. Arrowheads indicate normal stage-specific cavitation. (D) Transcript expression levels of genes that regulate pluripotency (*Nanog*, *Oct4*, and *Sox2*) and differentiation (*T/Brachyury*, mesoderm; *Gata4*, endoderm; *Hand1*, *Pax3*, and *nestin*, ectoderm; and *Cdx2*, trophoectoderm) were analyzed by quantitative RT-PCR. Error bars denote standard deviation; $n = 3$; *, $P < 0.05$. (E) The mRNA levels of *Nanog*, *Gata4*, *macroH2A1*, and *macroH2A2* were analyzed in ES cells expressing different hairpins directed against macroH2A1 and macroH2A2 at day 6 of EB formation (day 9 for *Nanog*). Error bars denote standard deviation; $n = 3$; *, $P < 0.05$.

which are tumors composed mainly of differentiated cells derived from all three germ layers. By injecting either sh-macroH2A1 or control mES cells, we observed that a loss of macroH2A1 provoked an obvious increase in teratoma growth (Fig. 5A). In addition to differentiated cells, teratomas generated from murine ES cells are known to contain a small proportion of malignant, undifferentiated carcinoma tissue (4). This primitive tissue was massively expanded in teratomas formed by macroH2A1-deficient mES cells (Fig. 5B). Importantly, the knockdown of macroH2A1 was sustained in these teratomas, albeit to a lesser extent than in the initial mES cell culture (Fig. 5C). Mesodermic cartilage, endodermic pulmonary epithelium, and neuronal tissues (including neuroglia) were the major differentiated representatives of the three germ layers in all teratomas, but their proportion was tendentially reduced in sh-macroH2A1 cell-derived teratomas (Fig. 5B). In line with these results, we found significantly increased mRNA levels of the pluripotency genes *Oct4* and *Sox2* in the bulk teratoma tissues derived from sh-macroH2A1 mES cells (Fig. 5C).

MacroH2A1 levels determine the differentiation propensity of PHKs. Having established a function for macroH2A in embryonic stem cells, we wished to address whether macroH2A has a similar regulatory function in adult stem cells. Staining of human scalp skin sections demonstrated that macroH2A1 is more highly expressed in the upper differentiated layers than in the basal cell layers that contain the stem cells and their activated progeny of transit-amplifying cells (Fig. 6A). Indeed, higher macroH2A1 lev-

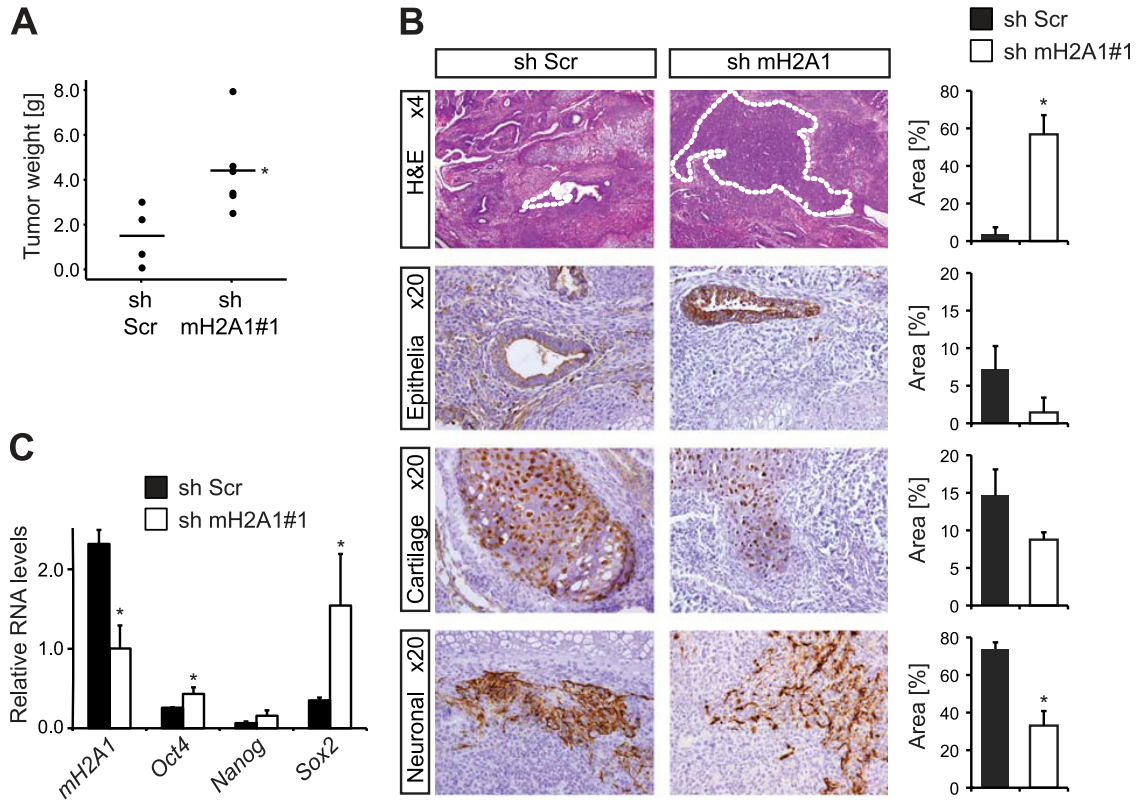

FIG 5 *In vivo* loss of macroH2A1 results in an expansion of malignant, undifferentiated carcinoma tissue. (A) Weight of teratomas generated by sh-macroH2A1 and control mES cells 3 weeks after injection.*, $P = 0.019$, as determined by nonparametric Mann-Whitney testing. (B) Hematoxylin-eosin (H&E) stainings and immunohistochemical analyses of teratoma sections. Malignant undifferentiated carcinoma tissues were identified by two independent pathologists and indicated by dotted lines. Different markers were used to stain tissues originating from all three lineages: S100 for cartilage (mesoderm), glial fibrilary acidic protein for neuroglia (ectoderm), and cytokeratins for epithelial cells (endoderm). Quantifications on the right were done on complete cross-sections of three samples. Error bars denote standard deviation; *, $P < 0.05$. (C) Quantitative RT-PCR analysis of RNA isolated from bulk teratoma tissue. Values are shown with respect to the mRNA levels in self-renewing stem cells, which were set to 1. Error bars denote standard deviation; $n = 3$; *, $P < 0.05$.

els correlate with the presence of the differentiation marker involucrin (Fig. 6B). Therefore, we turned to primary cultures of human keratinocytes (PHKs) derived from adult foreskin that express more macroH2A1 than macroH2A2 (Fig. 6C). Semiquantitative analysis of the relative RNA levels of all macroH2A forms suggests that macroH2A1.2 and macroH2A2 in an estimated ratio of 2:1 constitute the bulk amount of cellular macroH2A (Fig. 6D). The heterogeneous cultures of PHKs contain the stem cells of the interfollicular epidermis, as demonstrated by transplantation experiments that show that these specialized adult stem cells can give rise to all cell types of the skin (29). In culture, PHK cells grow into three-dimensional clones that differentiate from bottom to top. This differentiation process can be visualized by staining for involucrin, which is expressed in the upper layers formed by differentiated cells (Fig. 6E). Similar to the skin sections, macroH2A1 expression positively correlated with the differentiation of PHKs grown as colonies (Fig. 6E).

To study how the macroH2A1 level influences the differentiation process, we next generated PHKs that overexpressed the epitope-tagged macroH2A1.2 (Fig. 7A). When seeded at low cell numbers, the bulk of PHKs stop proliferating and differentiate, while only stem cells and late-derived, transit-amplifying cells are able to sufficiently self-renew to expand into holoclones (3). As shown in Fig. 7B, overexpression of macroH2A1.2 strongly reduced the number of holoclones. The overexpression of macroH2A1.1 and macroH2A2 had the same effect (data not shown). Importantly, overexpression of macroH2A did not affect the proliferation or survival of PHKs (data not shown). The observation that the level of the differentiation marker involucrin was increased in macroH2A1.2-overexpressing PHKs (Fig. 7C) further substantiated increased differentiation as the most likely mechanism for the observed reduction in colony formation (Fig. 7B). In the converse experiment, repression of macroH2A1 or macroH2A2 by stable shRNA interference increased the number of holoclones (Fig. 7D and E). Accordingly, cells with reduced macroH2A levels further displayed a reduction in involucrin mRNA levels (Fig. 7F). Together, these results suggest that macroH2A affects the balance of self-renewal and differentiation not only in ES cells but also in the adult stem cells of the interfollicular epidermis.

DISCUSSION

Here, we show that macroH2A plays a critical role in the differentiation of ES cells. Using shRNA-mediated knockdown, we studied the role that macroH2A plays in differentiation by three different approaches: RA-induced neuronal differentiation, EB formation, and *in vivo* differentiation in teratoma xenografts. We found that during neuronal differentiation and EB formation, macroH2A1 deficiency resulted in reduced or delayed activation of differentiation genes, many of which were shown to be direct

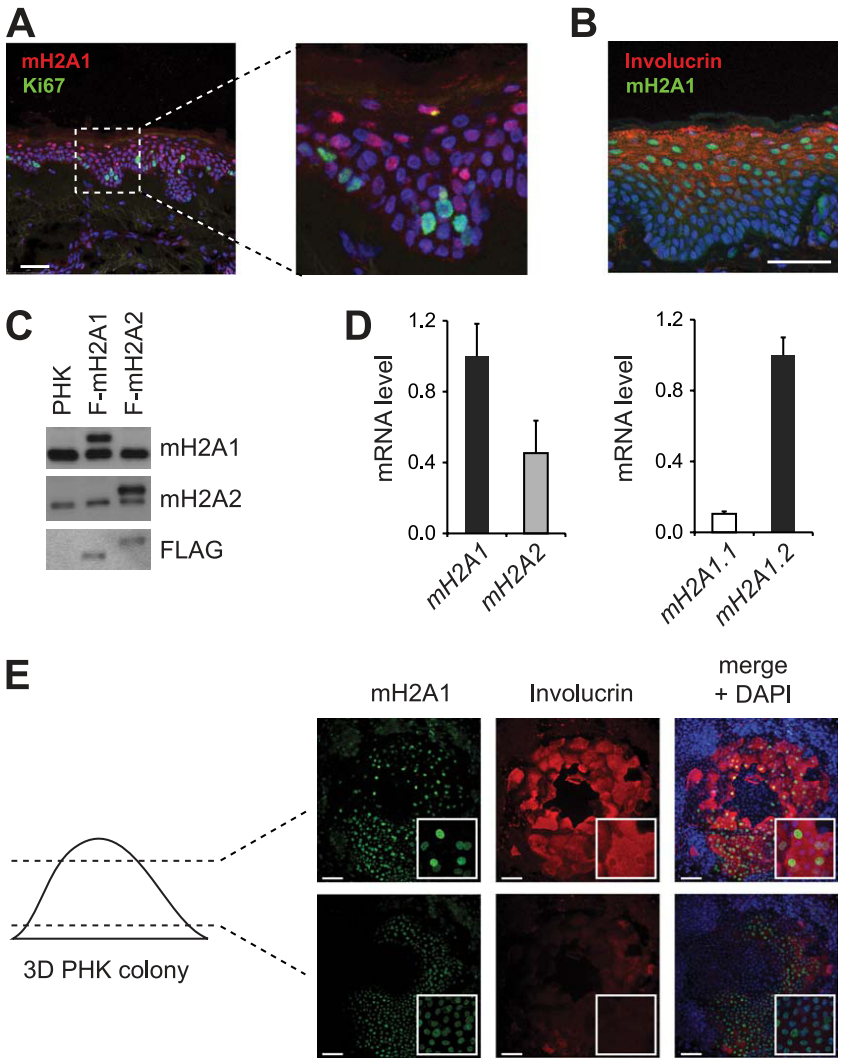

FIG 6 MacroH2A1 expression correlates with the differentiation of human keratinocytes. (A and B) Gradual upregulation of macroH2A1 from the basal to the more differentiated cell layers in a human scalp skin section, as shown by immunofluorescence. Cells were counterstained for the proliferation marker Ki67 (A) or the differentiation marker involucrin (B) and DAPI. Scale bars, 50 μm. (C) Lysates from primary human keratinocytes (PHKs) were analyzed by Western blotting together with extracts containing equivalent amounts of Flag (F)-tagged macroH2A1.2 and macroH2A2. (D) The relative mRNA levels of macroH2A forms were analyzed by quantitative RT-PCR and normalized to equimolar reference samples. (E) Confocal microscopy sections of a three-dimensional PHK colony. Involucrin was used to mark the differentiated cells present in the upper layer. DNA was counterstained with DAPI. Scale bars, 100 μm.

target genes of macroH2A1. Loss of macroH2A1 further resulted in the incomplete inactivation of the pluripotency genes that encode the key regulatory transcription factors Sox2, Nanog, and Oct4. In self-renewing stem cells, neither differentiation genes nor pluripotency genes were affected by the loss of macroH2A. Although macroH2A, and in particular macroH2A1.1, is known to inhibit proliferation in cancer cell lines (34), in mES cells macroH2A did not affect cell proliferation or viability. We conclude that macroH2A affects the differentiation but not the self-renewal of mES cells. Our data suggest that in ES cells macroH2A exerts its effect at least in part through a proactivating function on target genes, which include important regulators of differentiation (Fig. 7G). In teratoma xenografts, the reduction of macroH2A provoked a massive expansion of malignant, undifferentiated carcinoma tissue. This tissue is a minor but intrinsic component of mES cell-derived teratomas that consists of cells failing to enter differentiation (4). Taken together, our data suggest that macroH2A modulates the intricate balance between self-renewal and commitment to differentiation by contributing to the proper execution of differentiation programs.

Our data stand in direct contrast with a recent publication from Tanasijevic and Rasmussen, which reported that macroH2A had no influence on X chromosome inactivation or murine ES cell differentiation (41). This apparent discrepancy could be explained in several ways. First, the different genetic backgrounds of the ES cells used in the two studies might have influenced the penetrance and severity of the loss-of-function phenotype. It has long been known that different genetic backgrounds can impact the phenotype, and this is well documented for a large number of genes (32). Second, by relying on largely qualitative readouts and measurements at single time points during differentiation, the study by

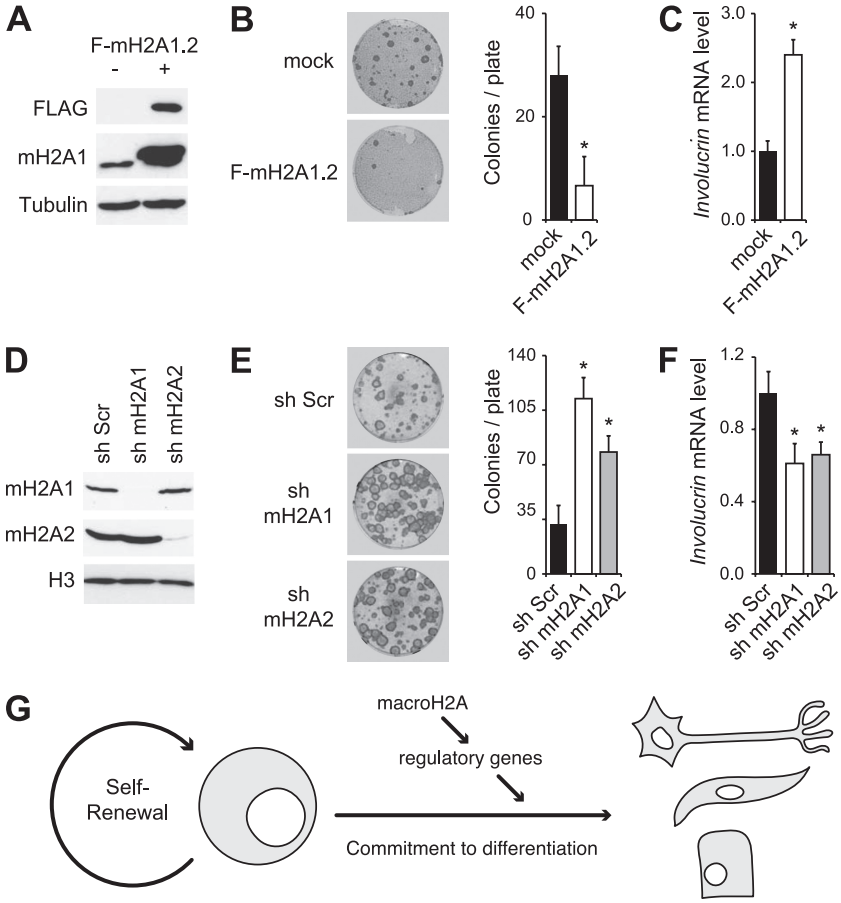

FIG 7 MacroH2A1 limits the self-renewal capacity, and favors the differentiation, of primary human keratinocytes. (A) Western blot analysis of lysates from PHKs overexpressing Flag (F)-tagged macroH2A1.2 using anti-FLAG, macroH2A1, and tubulin antibodies. (B) Colony formation analysis of the same PHKs grown on feeder cells. Error bars denote standard deviation; $n = 3$; *, $P < 0.05$. (C) The mRNA level of involucrin was analyzed by quantitative RT-PCR. Error bars denote standard deviation; $n = 3$; *, $P < 0.05$. (D) Efficient knockdown of macroH2A1 and macroH2A2 was assessed by Western blot. (E) Colony formation analysis of the same cells. Error bars denote standard deviation; $n = 3$; *, $P < 0.05$. (F) Expression analysis of involucrin by quantitative RT-PCR. Error bars denote standard deviation; $n = 3$; *, $P < 0.05$. (G) Cartoon illustrating how macroH2A affects the balance of self-renewal and differentiation. The presence of macroH2A on regulatory differentiation facilitates their activation and thereby the commitment of stem cells to differentiation.

Tanasijevic and Rasmussen might have missed the influence of macroH2A on the expression levels of differentiation genes that we observed by quantitative reverse transcriptase PCR (RT-PCR) at several, but not all, time points during differentiation. Furthermore, in xenografts, they showed that ES cells with strongly reduced macroH2A levels are able to form teratomas containing components of all three lineages (41). We corroborated this finding but also observed that primitive and poorly differentiated carcinoma tissue was strongly expanded in macroH2A1-deficient samples. Finally, we cannot exclude the possibility that the interfered ES cells used in the two studies might have differed in their residual macroH2A level to a point that could also explain the apparent discrepancies of the results.

Contradictory observations in macroH2A-deficient animals further fuel this controversy. In zebrafish, macroH2A2 knockdown provoked several developmental defects (10), while inactivation of the macroH2A1 gene in mice resulted in only mild phenotypes, including defects in lipid metabolism (6, 12). The knockout mice generated in different genetic backgrounds further differed in the severity of this metabolic defect. Boulard and colleagues observed a massive accumulation of fat (steatosis) in the livers of female animals, which was not reported by Changolkar and coworkers. Interestingly, this steatosis phenotype had a partial but stable penetrance of close to 50% in a mixed genetic background that was composed equally of two different mice strains (6). This suggests that the genetic background indeed strongly affects the impact of macroH2A1 deficiency.

Although macroH2A has long been considered to be a merely repressive chromatin mark, two publications have pointed out that, although macroH2A preferentially occupies repressed genes or genes with low transcriptional activity, it might actually be required to make these genes sensitive to activating cues. Thus, in HeLa cells, macroH2A1.1 was found to occupy the promoter of the *HSP70.1* gene and to be essential for its transcriptional activation in response to heat shock (35). Furthermore, macroH2A1 was shown to be required for the activation of a panel of direct target genes upon serum deprivation of MCF7 breast cancer cells (19). Our data now provide evidence for the physiological relevance of the still poorly recognized proactivating function of macroH2A in ES cell differentiation. In particular, we show that the presence of macroH2A1 on differentiation genes was required for their adequate induction while having no effect on basal activ-

ity. Our results thus extend the previous findings and further support the role of macroH2A in gene activation, which we suggest is at least partially responsible for its regulatory function during differentiation and developmental processes. The recent observation that macroH2A inhibited reprogramming by nuclear transfer (37) further suggests that macroH2A also contributes to the maintenance and stability of the differentiated epigenome.

The macroH2A1 ChIP-seq experiment reported here demonstrates that macroH2A1 marks genes encoding developmental regulators in mES cells and thus confirms previous results in human NT2/D1 cells (10). Taking into account that most macroH2A1 peaks were outside genes and that macroH2A-enriched regions were suggested to be large (13, 19, 30), it is perhaps more correct to state it the other way around: developmental genes tend to be embedded in macroH2A1-positive chromatin domains. The ChIP-seq analysis of macroH2A1 reported here, with its 15 million reads, was far from reaching saturation. Based on the particular distribution of macroH2A in large domains, we can extrapolate that two things would be needed to obtain saturation and thus full resolution and a comprehensive picture of genomic macroH2A1: first, a much larger number of reads, and second, improved antibodies that can generate ChIP data with better signal-to-noise ratios.

In order to fully understand the molecular aspects of macroH2A, we need to first understand how macroH2A-containing chromatin domains are established and how the presence of macroH2A and most likely its binding partners (of which only few have been determined so far) dictate the behavior of embedded genes. Furthermore, we will have to address the question of whether the correlation of macroH2A with differentiation is universal or, if instead, macroH2A regulates a limited number of specific lineage-choice decisions in early development and during adult tissue homeostasis.

ACKNOWLEDGMENTS

Work in the Buschbeck lab is supported by Spanish MICINN grants (SAF2009-08496 and RYC2010-07337). We are grateful for the following fellowship support: a postdoctoral FEBS fellowship for C.C., a predoctoral FPI fellowship (MICINN) for N.C., a predoctoral FI fellowship (AGAUR) for M.P., a postdoctoral Beatriu de Pinós contract (AGAUR) for J.D., and the Ramón y Cajal fellowship (MICINN) for M.B.

We thank Iris Uribesalgo and Didier Auboeuf for critically reading the manuscript, Gloria Pascual, Anna Palau, Roberto Malinverni, Martin Lange, and Lluís Morey for advice and help, and Andreas Ladurner and Gideon Dreyfuss for providing reagents.

REFERENCES

1. **Agelopoulos M, Thanos D.** 2006. Epigenetic determination of a cell-specific gene expression program by ATF-2 and the histone variant macroH2A. EMBO J. **25**:4843–4853.
2. **Barde I, Salmon P, Trono D.** 2010. Production and titration of lentiviral vectors. Curr. Protoc. Neurosci. **53**:4.21.1–4.21.23.
3. **Barrandon Y, Green H.** 1987. Three clonal types of keratinocyte with different capacities for multiplication. Proc. Natl. Acad. Sci. U. S. A. **84**: 2302–2306.
4. **Blum B, Bar-Nur O, Golan-Lev T, Benvenisty N.** 2009. The anti-apoptotic gene survivin contributes to teratoma formation by human embryonic stem cells. Nat. Biotechnol. **27**:281–287.
5. **Boix R, et al.** 2009. Primary renal cell carcinoma in a transplanted kidney: genetic evidence of recipient origin. Transplantation **87**:1057–1061.
6. **Boulard M, et al.** 2010. Histone variant macroH2A1 deletion in mice causes female-specific steatosis. Epigenetics Chromatin. **3**:8.
7. **Buschbeck M, Di Croce L.** 2010. Approaching the molecular and physiological function of macroH2A variants. Epigenetics **5**:118–123.
8. **Buschbeck M, Hofbauer S, Croce LD, Keri G, Ullrich A.** 2005. Abl-kinase-sensitive levels of ERK5 and its intrinsic basal activity contribute to leukaemia cell survival. EMBO Rep. **6**:63–69.
9. **Buschbeck M, et al.** 2007. PML4 induces differentiation by Myc destabilization. Oncogene **26**:3415–3422.
10. **Buschbeck M, et al.** 2009. The histone variant macroH2A is an epigenetic regulator of key developmental genes. Nat. Struct. Mol. Biol. **16**:1074–1079.
11. **Chakravarthy S, et al.** 2005. Structural characterization of the histone variant macroH2A. Mol. Cell. Biol. **25**:7616–7624.
12. **Changolkar LN, et al.** 2007. Developmental changes in histone macroH2A1-mediated gene regulation. Mol. Cell. Biol. **27**:2758–2764.
13. **Changolkar LN, et al.** 2010. Genome-wide distribution of macroH2A1 histone variants in mouse liver chromatin. Mol. Cell. Biol. **30**:5473–5483.
14. **Dai B, Rasmussen TP.** 2007. Global epiproteomic signatures distinguish embryonic stem cells from differentiated cells. Stem Cells **25**:2567–2574.
15. **Durinck S, Spellman PT, Birney E, Huber W.** 2009. Mapping identifiers for the integration of genomic datasets with the R/Bioconductor package biomaRt. Nat. Protoc. **4**:1184–1191.
16. **Evans MJ, Kaufman MH.** 1981. Establishment in culture of pluripotential cells from mouse embryos. Nature **292**:154–156.
17. **Feldman N, et al.** 2006. G9a-mediated irreversible epigenetic inactivation of Oct-3/4 during early embryogenesis. Nat. Cell Biol. **8**:188–194.
18. **Frank SR, Schroeder M, Fernandez P, Taubert S, Amati B.** 2001. Binding of c-Myc to chromatin mediates mitogen-induced acetylation of histone H4 and gene activation. Genes Dev. **15**:2069–2082.
19. **Gamble MJ, Frizzell KM, Yang C, Krishnakumar R, Kraus WL.** 2010. The histone variant macroH2A1 marks repressed autosomal chromatin, but protects a subset of its target genes from silencing. Genes Dev. **24**:21–32.
20. **Gentleman RC, et al.** 2004. Bioconductor: open software development for computational biology and bioinformatics. Genome Biol. **5**:R80.
21. **Heath JK, Smith AG.** 1988. Regulatory factors of embryonic stem cells. J. Cell Sci. Suppl. **10**:257–266.
22. **Hemberger M, Dean W, Reik W.** 2009. Epigenetic dynamics of stem cells and cell lineage commitment: digging Waddington's canal. Nat. Rev. Mol. Cell Biol. **10**:526–537.
23. **Hernandez-Munoz I, et al.** 2005. Stable X chromosome inactivation involves the PRC1 Polycomb complex and requires histone MACROH2A1 and the CULLIN3/SPOP ubiquitin E3 ligase. Proc. Natl. Acad. Sci. U. S. A. **102**:7635–7640.
24. **Honma M, Benitah SA, Watt FM.** 2006. Role of LIM kinases in normal and psoriatic human epidermis. Mol. Biol. Cell **17**:1888–1896.
25. **Hooper M, Hardy K, Handyside A, Hunter S, Monk M.** 1987. HPRT-deficient (Lesch-Nyhan) mouse embryos derived from germline colonization by cultured cells. Nature **326**:292–295.
26. **Huang DW, Sherman BT, Lempicki RA.** 2009. Systematic and integrative analysis of large gene lists using DAVID bioinformatics resources. Nat. Protoc. **4**:44–57.
27. **Kapoor A, et al.** 2010. The histone variant macroH2A suppresses melanoma progression through regulation of CDK8. Nature **468**:1105–1109.
28. **Langmead B, Trapnell C, Pop M, Salzberg SL.** 2009. Ultrafast and memory-efficient alignment of short DNA sequences to the human genome. Genome Biol. **10**:R25.
29. **Lichti U, Anders J, Yuspa SH.** 2008. Isolation and short-term culture of primary keratinocytes, hair follicle populations and dermal cells from newborn mice and keratinocytes from adult mice for in vitro analysis and for grafting to immunodeficient mice. Nat. Protoc. **3**:799–810.
30. **Mietton F, et al.** 2009. Weak but uniform enrichment of the histone variant macroH2A1 along the inactive X chromosome. Mol. Cell. Biol. **29**:150–156.
31. **Morey L, et al.** 2012. Non-overlapping function of the Polycomb group Cbx family of proteins in embryonic stem cells. Cell Stem Cell **10**:47–62.
32. **Muller U.** 1999. Ten years of gene targeting: targeted mouse mutants, from vector design to phenotype analysis. Mech. Dev. **82**:3–21.
33. **Niwa H.** 2007. How is pluripotency determined and maintained? Development **134**:635–646.
34. **Novikov L, et al.** 2011. QKI-mediated alternative splicing of the histone variant macroH2A1 regulates cancer cell proliferation. Mol. Cell. Biol. **31**:4244–4255.
35. **Ouararhni K, et al.** 2006. The histone variant mH2A1.1 interferes with transcription by down-regulating PARP-1 enzymatic activity. Genes Dev. **20**:3324–3336.
36. **Pasini D, Bracken AP, Jensen MR, Lazzerini Denchi E, Helin K.** 2004. Suz12 is essential for mouse development and for EZH2 histone methyltransferase activity. EMBO J. **23**:4061–4071.
37. **Pasque V, Gillich A, Garrett N, Gurdon JB.** 2011. Histone variant

macroH2A confers resistance to nuclear reprogramming. EMBO J. **30**: 2373–2387.
38. **Pehrson JR, Costanzi C, Dharia C.** 1997. Developmental and tissue expression patterns of histone macroH2A1 subtypes. J. Cell Biochem. **65**: 107–113.
39. **Sarma K, Reinberg D.** 2005. Histone variants meet their match. Nat. Rev. Mol. Cell Biol. **6**:139–149.
40. **Sporn JC, et al.** 2009. Histone macroH2A isoforms predict the risk of lung cancer recurrence. Oncogene **28**:3423–3428.
41. **Tanasijevic B, Rasmussen TP.** 2011. X chromosome inactivation and differentiation occur readily in ES cells doubly-deficient for macroH2A1 and macroH2A2. PLoS One **6**:e21512.
42. **Uribesalgo I, et al.** 2011. E-box-independent regulation of transcription and differentiation by MYC. Nat. Cell Biol. **13**:1443–1449.
43. **Xu H, et al.** 2010. A signal-noise model for significance analysis of ChIP-seq with negative control. Bioinformatics **26**:1199–1204.
44. **Zhang Y, et al.** 2008. Model-based analysis of ChIP-Seq (MACS). Genome Biol. **9**:R137.
45. **Zhu LJ, et al.** 2010. ChIPpeakAnno: a Bioconductor package to annotate ChIP-seq and ChIP-chip data. BMC Bioinformatics **11**:237.